Since the observed fundamental at 2085 cm^{-1} is a mixture of ketene-like C=C and C=O stretches, it is of interest to see what other fundamentals these two internal coordinates affect. The remainder of the C=O stretch goes primarily (i.e., 31%) into the a_1 mode predicted at 1770 cm^{-1} (DZP MP2). If we decrease this theoretical harmonic frequency for anharmonicity, basis set, and higher level correlation effects, the fundamental vibrational frequency may be estimated to be about 1650 cm^{-1}. Note that the IR intensity of this fundamental is predicted to be substantial, 24 km/mol, but nothing like the 1017 km/mol of the feature observed near 2085 cm^{-1}.

A final point of particular interest is the feature at 2093 cm^{-1} long assigned[5] to the C≡C stretch of perdeuterated benzyne. Note that in an N_2 matrix at 12 K, the shift in this frequency was determined by Dunkin and MacDonald to be 2093 - 2084 = 9 cm^{-1}. It would not be surprising at this point to conclude that this feature is instead a ketene-like fundamental of perdeuterated CPDK. However, this harmonic vibrational frequency is predicted to be red-shifted by 0.5 cm^{-1} at the DZ+P SCF level of theory and by 0.3 cm^{-1} with the DZ+P MP2 method. Thus we must be very cautious in assigning the experimental IR feature at 2093 cm^{-1}. New experiments might be very helpful in this regard.

Concluding Remarks

This work provides a complete theoretical prediction of the harmonic vibrational frequencies and infrared intensities of the cyclopentadienylideneketene molecule (3). Until recently[16,18] there was no evidence that this molecule had been observed spectroscopically. However the theoretical normal mode that is 49% ketene C=C stretch and 40% C=O stretch is predicted to have a remarkably strong IR intensity. These predictions are consistent with the observed IR feature at 2085 cm^{-1}, which was for many years assumed to be due to the C≡C stretch in benzyne.

Further experimental studies of 3 would be of great value, as this new molecule becomes of interest in its own right. An obvious question yet to be resolved is whether some of the other fundamentals previously assigned[4-9] to benzyne are in fact due to cyclopentadienylideneketene. For cyclopentadienylideneketene (3) the next most intense IR feature is predicted at 772 cm^{-1} (harmonic vibrational frequency, b_1 symmetry, intensity 92.7 km/mol, DZP MP2). This theoretical result fits well with the observed "benzyne" feature[4] at 736 cm^{-1}, which is the strongest experimental IR feature after that at 2085 cm^{-1}. Unfortunately, this interpretation is muddied by the fact that benzyne itself has its very strongest IR fundamental predicted at 751 cm^{-1} (b_1 symmetry, 85.8 km/mol, DZP MP2). Thus the theoretical predictions for either cyclopentadienylideneketene or benzyne can accommodate the intense IR feature observed at 736 cm^{-1}.

Acknowledgment. This research was supported by the U.S. Department of Energy, Office of Basic Energy Sciences, Division of Chemical Sciences, Fundamental Interactions Branch (Grant DE-FG09-87ER13811). We thank Drs. Mary M. Gallo and Yaoming Xie for helpful discussions.

Registry No. Cyclopentadienylideneketene, 115252-80-7.

Calculation of the Relative Binding Free Energy of Three Inhibitors of the Photosynthetic Reaction Center of *Rhodopseudomonas viridis* Using the Molecular Dynamics/Free Energy Perturbation Method

John E. Mertz,[†] Jan W. Andzelm,[†] Detlef Labrenz,[‡] and Ursula Egner*[,§]

Contribution from Cray Research, Inc., 655E Lone Oak Drive, Eagan, Minnesota 55120, Cray Research GmbH, Kistlerhofstrasse 168, D-8000 München 70, Germany, and Schering AG, Müllerstrasse 170-178, D-1000 Berlin 65, Germany. *Received September 9, 1991*

Abstract: The results of the relative changes in binding free energy between the complex of the bacterial photosynthetic reaction center (RC) of *Rhodopseudomonas viridis* with inhibitors ametryn, atraton, and prometon are presented. These results were determined by using molecular dynamics, free energy perturbation methods. Force field parameters for the cofactors and non-heme iron of the RC along with the inhibitors are developed from a combination of quantum mechanical calculations and previous spectroscopic and molecular modeling studies. The calculated free energy changes compare well with the measured data and lie within the error limits of this method. The calculations yielded a ranking of the relative stabilities of the inhibitors as atraton < prometon < ametryn. The relative free energy of solvation and the relative free energy of the complexes between the inhibitors and the RC both favor a hydrophobic substituent for better binding.

Introduction

The photosynthetic reaction center (RC) complexes provide model systems for rationalizing the ability of various herbicides to inhibit photosynthesis. RCs have been purified from numerous species of bacteria, and the X-ray structures of the RCs of *Rhodopseudomonas viridis* (*Rps. viridis*) and *Rhodobacter sphaeroides* (*Rb. sphaeroides*) have been solved to high resolution.[1-3] RCs from many species are composed of three protein subunits (L, M, and H), four bacteriochlorophylls, two bacteriopheophytins, two quinones (Q_A and Q_B), and one non-heme iron atom. In the case of the RC of *Rps. viridis*, a cytochrome with four heme molecules is also present. Since the elucidation of the X-ray structure of these RCs, several calculations have been carried out that relate their structure and function. Simulations of optical spectra were performed including absorption, light-induced absorbence changes, and circular dichroism.[4-7] The

[†] Cray Research, Inc.
[‡] Cray Research GmbH.
[§] Schering AG.

(1) Deisenhofer, J.; Epp, O.; Miki, K.; Huber, R.; Michel, H. *Nature* **1985**, *318*, 618.
(2) Allen, J. P.; Feher, G.; Yeates, T. O.; Komiya, H.; Rees, D. C. *Proc. Natl. Acad. Sci. U.S.A.* **1988**, *85*, 8487.
(3) Creighton, S.; Hwang, J.-K.; Warshel, A.; Parson, W. W.; Norris, J. *Biochemistry* **1988**, *27*, 774.

0002-7863/92/1514-4762$03.00/0 © 1992 American Chemical Society

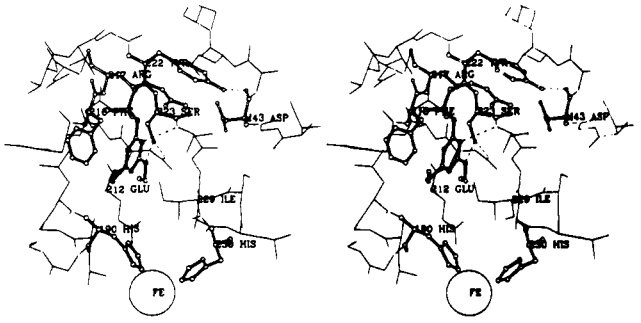

Figure 1. Stereo presentation of the binding of the triazine herbicide terbutryn to the active site of the L subunit of the RC of *Rps. viridis*. The inhibitor forms two hydrogen bonds with the protein (drawn in dashed lines). This plot was taken from the X-ray structure of the complex and was provided by Dr. I. Sinning.

mechanism of the initial electron-transfer process was examined by dynamics simulations for *Rb. sphaeroides*[3] and *Rps. viridis*.[8]

Bacterial RCs are mainly sensitive to herbicides of the triazine family[9,10] although recently a mutant of the RC of *Rps. viridis* was found that is sensitive to diuron, a urea-type herbicide.[11] These herbicides function by blocking the electron flow between the acceptor and the donor quinones (Q_A and Q_B, respectively). Since the X-ray crystallographic structures of the RC from *Rps. viridis* binding the herbicides terbutryn (2-(methylthio)-4-(ethylamino)-6-(*tert*-butylamino)-*s*-triazine) or *o*-phenanthroline can be obtained,[12] the RC of this purple bacteria is well suited to study the effects of herbicide binding. The binding free energies for several triazines, both in isolated RCs and in chromatophores, have been determined from I_{50} values (i.e., the concentration of the herbicide which inhibits 50% of the electron flow).[10,11] Terbutryn, like other triazines, is a competitive inhibitor to the secondary quinone Q_B and replaces it from the active site of the L subunit of the RC. The X-ray structure analysis of the complex between the RC and terbutryn reveals that this herbicide forms two hydrogen bonds with the L subunit: the hydrogen of the ethylamino nitrogen interacts with the O_γ of Ser L223, and the 3-nitrogen of the triazine ring interacts with the peptide NH of Ile L224. The methylthio group is tightly bound between the hydrophobic residues Leu L189 and Ile L229; see Figure 1.

The purpose of this work is to understand how different substituents influence the binding modes of the triazines in *Rps. viridis*. To do this, we calculated the relative free energy of binding for three of the herbicides in the family of symmetric triazines (see Figure 2) using molecular dynamics (MD), free energy perturbation (FEP) methods.[13-15] Considerable effort was put

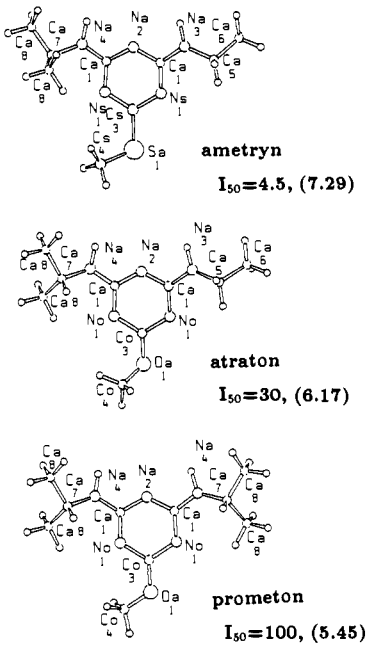

Figure 2. Structure and I_{50} values of the triazines studied in this analysis. The atoms are marked with the atom types used in the parametrization. The I_{50} values (concentration of herbicide where 50% of the electron transport is inhibited) were determined in chromatophores (in μM); $\Delta G°$ values are given in parentheses (in kcal/mol). All stereo plots were done by SCHAKAL.[45]

forth to obtain physically reasonable force field parameters for this system. These parameters were obtained from a combination of quantum mechanical calculations and previous spectroscopic and molecular modeling studies. It is worth noting that in this study the parameter development and calculation of the binding free energies were carried out *before* the experimental I_{50} values were measured.

Force Field Parametrization

The MD simulation of the RC of *Rps. viridis* with its cofactors and inhibitors provides a challenging task in force field parameter development. The parameter sets were developed for the AMBER[16,17] force field, and the nonbonded parameters used in the simulation were transferred directly from Weiner et al.[16] This was done to produce consistent nonbonded interactions within the entire system: cofactors, inhibitors, and protein. The partial charges were obtained using a procedure modeled after the electrostatic potential (ESP) fitting process described by Singh and Kollman.[18] In this method, the quantum mechanical ESP is calculated on a set of grid points that represent the surface of the molecule. Then the ESP due to the partial charges centered on the nuclei is also calculated on the points of this grid. The difference between these two potentials is minimized by adjusting the partial charges through a least-squares fit. The quantum mechanical electrostatic potential was obtained using local spin density (LSD) methods. These calculations were performed using the density functional program DGauss.[19] The DGauss methodology is based on analytical variational fitting of electron density using Gaussian-type orbitals. The exchange–correlation potential is approximated using a fitting procedure that involves numerical integration. All calculations, unless otherwise noted, were performed at the basis set level of 6-31G**.[20] LSD methods allow

(4) Won, Y.; Friesner, R. A. *J. Phys. Chem.* **1988**, *92*, 2208.
(5) Zinth, W.; Knapp, E. W.; Fischer, S. F.; Kaiser, W.; Deisenhofer, J.; Michel, H. *Chem. Phys. Lett.* **1985**, *119*, 1.
(6) Parson, W. W.; Warshel, A. *J. Am. Chem. Soc.* **1987**, *109*, 6152.
(7) Zengh, C.; Davis, M. E.; McCammon, J. A. *Chem. Phys. Lett.* **1990**, *173*, 246.
(8) Treutlein, H.; Schulten, K.; Deisenhofer, J.; Michel, H.; Brünger, A.; Karplus, M. *The Photosynthetic Reaction Center. Structure and Dynamics*; Breton, J., Vermeglio, A., Eds.; NATO ASI Series 149; Plenum: New York, 1989; pp 139–150.
(9) Stein, R. R.; Castellvi, A. L.; Bogacz, J. P.; Wraight, C. A. *J. Cell. Biochem.* **1984**, *24*, 243.
(10) Sinning, I.; Michel, H. *Z. Naturforsch.* **1987**, *42c*, 751.
(11) Sinning, I.; Michel, H.; Mathis, P.; Rutherford, A. W. *FEBS Lett.* **1989**, *256*, 192.
(12) Michel, H.; Epp, O.; Deisenhofer, J. *EMBO J.* **1986**, *5*, 2445.
(13) Lybrand, T. P.; McCammon, J. A.; Wippf, G. *Proc. Natl. Acad. Sci. U.S.A.* **1986**, *83*, 833.
(14) Bash, P. A.; Singh, U. C.; Langridge, R.; Kollman, P. A. *Science* **1987**, *236*, 564.
(15) McCammon, J. A.; Harvey, S. C. *Dynamics of Proteins and Nucleic Acids*; Cambridge University Press: New York, 1987; Chapter 4. Brooks, C. L., III; Karplus, M.; Pettitt, B. M. *Proteins: A Theoretical Perspective of Dynamics, Structure, and Thermodynamics*; Advances in Chemical Physics Vol. LXXI; John Wiley & Sons: New York, 1988; Chapter 5. *Computer Simulation of Biomolecular Systems: Theoretical and Experimental Applications*; van Gunsteren, W., Weiner, P., Eds.; Escom Science Publishers: Leiden, 1989; pp 1–148. Saqi, M. A. S.; Goodfellow, J. M. *Protein Eng.* **1990**, *5*, 419.
(16) Weiner, S. J.; Kollman, P. A.; Case, D. A.; Singh, U. C.; Ghio, C.; Alagona, G.; Profeta, S.; Weiner, P. *J. Am. Chem. Soc.* **1984**, *106*, 765.
(17) Singh, U. C.; Weiner, P. K.; Caldwell, J. W.; Kollman, P. A. *AMBER (UCSF)*, Version 3.0; Department of Pharmaceutical Chemistry, University of California: San Francisco, 1986.
(18) Singh, U. C.; Kollman, P. A. *J. Comput. Chem.* **1984**, *5*, 129.
(19) Andzelm, J. W. In *Density Functional Methods in Chemistry*; Labanowski, J. K., Andzelm, J. W., Eds.; Springer-Verlag: New York, 1991; Chapter 11. Wimmer, E. *Ibid.*; Chapter 2.

Table I. Additional Bond Parameters[a]

bond	K_r	r_{eq}	bond	K_r	r_{eq}
C-CR2	410	1.444	CQ8-CQ8	438.21	1.407
C-CT	317	1.51	CQ8-CQ9	453.65	1.393
C-OF1	656	1.25	CQ9-CQ10	452.38	1.383
C-OS	320	1.41	CQ9-HQ9	354.70	1.080
CA1-NA2	490.26	1.325	CQ10-CQ10	453.65	1.401
CA1-NA3	511.46	1.338	CQ10-HQ10	354.70	1.080
CA1-NA4	511.46	1.338	CQ12-HQ12	336.9	1.09
CA1-NO1	531.81	1.331	CR-NFL	477	1.343
CA1-NS1	446.55	1.334	CR-NFU	477	1.343
CA5-CA6	275.09	1.529	CR1-CR2	379	1.440
CA5-HA5	362.78	1.085	CR1-CR3	502	1.383
CA5-NA3	320.14	1.455	CR1-CT	317	1.504
CA6-HA6	407.74	1.087	CR1-NR1	406	1.380
CA7-CA8	226.74	1.546	CR1-NR2	406	1.380
CA7-HA7	329.87	1.128	CR2-CR	317	1.495
CA7-NA4	304.25	1.474	CR2-CR2	512	1.352
CA8-HA8	376.25	1.109	CR2-CR4	410	1.444
CO3-NO1	448.38	1.316	CR2-CR5	379	1.440
CO3-OA1	514.69	1.317	CR3-CR5	502	1.383
CO4-HO4	441.48	1.080	CR3-CT	317	1.510
CO4-OA1	359.86	1.413	CR3-HR3	361	1.090
CQ1-CQ2	314.3	1.54	CR4-O	570	1.229
CQ1-CQ5	314.3	1.54	CR4-CT	317	1.51
CQ1-CT	310	1.526	CR5-NR2	406	1.380
CQ1-HQ1	324.3	1.09	CS3-NS1	512.67	1.316
CQ2-CQ3	334.9	1.54	CS3-SA1	288.77	1.760
CQ2-CQ4	566.4	1.33	CS4-SA1	209.12	1.808
CQ3-HQ3	336.9	1.09	CS4-HS4	413.25	1.080
CQ4-CQ5	314.3	1.54	CW-NFL	427	1.381
CQ4-HQ4	354.7	1.09	CW-NFU	427	1.381
CQ5-CQ6	334.9	1.54	FE-NFL	246.8	1.95
CQ5-HQ5	324.3	1.09	FE-NFU	383.3	1.86
CQ5-OS	320	1.41	FE-OF1	344.7	1.96
CQ6-CQ6	595.27	1.340	HA3-NA3	618.44	0.992
CQ6-CQ7	321.00	1.478	HA4-NA4	536.08	1.009
CQ6-CQ12	334.9	1.54	HR2-NR2	432.70	1.01
CQ7-CQ8	321.00	1.468	MG-NR1	121	2.081
CQ7-OQ7	740.51	1.223	MG-NR2	121	2.081

[a] For the potential $K_r(r - r_{eq})^2$ where K_r is in kcal/mol·Å^2 and r_{eq} is in Å.

us to obtain partial charges on molecular fragments that are too large for feasible computation, but are quantitatively comparable to Hartree–Fock (HF) methods.[21] Another motivation is that recent studies have shown LSD methods to be successful in calculating electronic and geometrical properties of organometallic compounds.[22] The partial charges and the equivalent AMBER nonbonded atom types for all inhibitors and ligands are given in the supplementary material.[23] The internal parameters (e.g., bond, angle, and torsion) were obtained from a combination of quantum mechanical calculations, valence force fields derived from spectroscopic data, and data from Weiner et al.[16] The parameters for these interactions are given in Tables I–IV, and the corresponding atom symbols are displayed in Figures 2, 4, and 5. The details of the generation of these parameters are explained below.

Inhibitors. The internal force field parameters used to describe the inhibitors (Figure 2) were obtained by minimizing the difference between the first and second derivatives of HF and force field potential energy surfaces.[24] We used the GRADSCF[25] program to carry out the HF calculations, and the least-squares fit was performed by the suite of programs developed at Biosym Technologies, Inc.[26] For computational efficiency, the potential

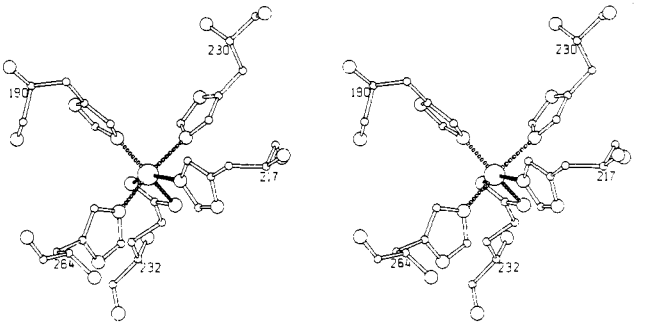

Figure 3. Stereo presentation of the amino acid residues interacting with the non-heme iron atom in the RC of *Rps. viridis*: the four histidines, L190, L230, M217, and M264, and the glutamic acid, M232.

surfaces of the inhibitors were modeled by four molecular fragments: ethylamine, isopropylamine, methoxytriazine, (methylthio)triazine. Each of these molecules had its geometry optimized at the basis set level of 6-31G*. Once the equilibrium geometries were computed, other nonequilibrium configurations were generated by slightly distorting the positions of the nuclei. The distortions were carried out randomly and resulted in bond lengths and bond angles that deviated from the equilibrium geometry by ±0.02 Å and ±2.5°, respectively. Torsional angles were chosen to adequately sample configurations available to the molecules at room temperature. The total number of configurations used in the fit was 33. Initially, cubic and quadratic terms were added to the bond and angle bending terms to improve the convergence of the fit. Once convergence was obtained, the harmonic terms were used as initial guesses as to the final harmonic fit. This procedure yielded all of the internal parameters for the inhibitor molecules with the exception of one angle, three proper torsions, and one improper torsion. These values were transferred from similar interactions found in Weiner et al.[16]

Non-Heme Iron Atom. The goal of the parameter development of the non-heme iron complex was to produce physically realistic internal parameters and pair potentials that were based upon quantum mechanical calculations. In the RC, the iron atom is complexed with four histidines, L190, L230, M217, M264, and one glutamic acid, M232. The model system chosen to study the iron complex contained the Fe^{2+} ion, four methylimidazoles, and one negatively charged propanoic acid (the X-ray structure is shown in Figure 3). The overall charge of the complex was +1, and the calculated spin state ($S = 2$) was found to be consistent with experimental studies.[27] In the following, a summary of the quantum mechanical calculations is presented; a detailed description of the calculations will appear elsewhere.[28]

The first step in the parametrization was to obtain a molecular geometry that was close to the X-ray structure, but at a local minimum in energy. Initially, the methylimidazole and the propanoic acid were optimized separately at the semiempirical level using the AM1 Hamiltonian in MOPAC.[29] These fragments were kept frozen during the remaining optimization procedure. Then the internal coordinates (bonds, angles, and dihedrals), which contained the Fe^{2+} atom, were optimized using the PRDDO program.[30] A final optimization of these internal coordinates was done by the DGauss program.[19] For the Fe atom, an all-electron, valence, triple-zeta basis set[31] was used, and a 6-31G** basis set was used for the remaining atoms. In total, there were 595 basis functions. After the equilibrium structure was found, harmonic force constants for the bond-stretching terms were calculated using a finite difference method. In this calculation

(20) Hehre, W. J.; Ditchfield, R.; Pople, J. A. *J. Chem. Phys.* **1972**, *56*, 2257. Hariharan, P. C.; Pople, J. A. *Theo. Chim. Acta* **1973**, *28*, 213.
(21) Mertz, J. E.; Andzelm, J. W.; Wimmer, E.; Lybrand, T. L. *J. Comput. Chem.*, submitted for publication.
(22) *Density Functional Methods in Chemistry*; Labanowski, J. K., Andzelm, J. W., Eds.; Springer-Verlag: New York, 1991; references therein.
(23) Supplementary material is the input files to the AMBER PREP module.
(24) Maple, J. R.; Dinur, U.; Hagler, A. T. *Proc. Natl. Acad. Sci. U.S.A.* **1985**, *15*, 5350.
(25) Kormornicki, A. *GRADSCF*; Polyatomic Research Institute, Mountain View, CA, 1985.
(26) Biosym Technologies, Inc., San Diego, CA 92121.
(27) Butler, W. F.; Johnston, D. C.; Shore, H. B.; Fredkin, D. R.; Okamura, M. Y.; Feher, G. *Biophys. J.* **1980**, *32*, 967.
(28) Andzelm, J. W.; Egner, U.; Mertz, J. E.; Labrenz, D.; Wimmer, E. Manuscript in preparation.
(29) MOPAC (5.01): Stewart, J. J. P., QCPE, No. 455.
(30) Marynick, D. S.; Libscomb, W. N. *Proc. Natl. Acad. Sci. U.S.A.* **1982**, *79*, 1341.
(31) Andzelm, J. W.; Radzio, E.; Salahub, D. R. *J. Comput. Chem.* **1985**, *6*, 520.

Table II. Additional Angle Parameters[a]

angle	K_θ	θ_0	angle	K_θ	θ_0	angle	K_θ	θ_0
C–CR2–CR1	80.0	128.0	CQ6–CQ12–HQ12	43.9	109.5	CR5–CR3–CT	75.0	106.4
C–CR2–CR2	70.0	125.2	CQ7–CQ6–CQ12	65.2	119.4	CR5–NR2–HR2	20.6	127.6
C–CT–CR3	75.0	108.92	CQ7–CQ8–CQ8	43.6	120.0	CR5–NR2–MG	21.6	127.6
C–CT–CR4	63.0	111.1	CQ7–CQ8–CQ9	58.0	120.3	CS3–SA1–CS4	126.73	102.35
C–OS–CQ5	60.0	109.5	CQ8–CQ7–OQ7	76.5	121.5	CT–C–OF1	70.0	117.0
C–OS–CT	60.0	109.5	CQ8–CQ8–CQ9	49.9	119.7	CT–C–OS	80.0	119.8
CA1–NA2–CA1	70.69	114.05	CQ8–CQ9–CQ10	61.3	120.2	CT–CQ1–HQ1	47.8	109.5
CA1–NA3–CA5	70.69	120.0	CQ8–CQ9–HQ9	34.1	119.9	CT–CR1–NR1	80.0	113.2
CA1–NA3–HA3	44.80	120.0	CQ9–CQ10–CQ10	61.3	120.1	CT–CR4–O	80.0	120.0
CA1–NA4–CA7	70.69	120.0	CQ9–CQ10–HQ10	34.1	119.9	HA4–NA4–HA4	45.54	104.62
CA1–NA4–HA4	44.80	120.0	CQ10–CQ10–HQ10	35.0	120.0	HA5–CA5–HA5	37.75	106.32
CA1–NO1–CO3	87.28	113.82	CO3–OA1–CO4	77.94	119.3	HA5–CA5–NA3	42.85	107.69
CA1–NS1–CS3	75.54	113.91	CR–NFL–CW	70.0	120.0	HA6–CA6–HA6	33.37	107.82
CA5–CA6–HA6	47.68	111.08	CR–NFU–CW	70.0	120.0	HA7–CA7–NA4	66.06	110.31
CA5–NA3–HA3	55.53	110.66	CR1–CR2–CR2	98.5	106.8	HA8–CA8–HA8	41.42	107.48
CA6–CA5–HA5	51.27	109.62	CR1–CR2–CT	70.0	128.0	HC–CR–NFL	35.0	120.0
CA6–CA5–NA3	98.58	115.49	CR1–CR3–CR1	104.3	121.4	HC–CR–NFU	35.0	120.0
CA7–CA8–HA8	54.14	111.39	CR1–CR3–CR5	104.3	125.4	HC–CW–NFL	35.0	120.0
CA7–NA4–HA4	62.45	109.56	CR1–CR3–CT	70.0	128.1	HC–CW–NFU	35.0	120.0
CA8–CA7–CA8	78.51	112.62	CR1–CR3–HR3	33.2	119.3	HO4–CO4–OA1	44.59	109.5
CA8–CA7–HA7	61.12	106.96	CR1–CT–CT	63.0	110.1	HO4–CO4–HO4	38.86	109.5
CA8–CA7–NA4	88.77	109.94	CR1–CT–HC	35.0	109.5	HQ1–CQ1–HQ1	38.8	109.5
CC–CW–NFL	70.0	120.0	CR1–NR1–CR1	110.0	104.8	HQ3–CQ3–HQ3	38.0	109.5
CC–CW–NFU	70.0	120.0	CR1–NR1–MG	21.6	127.6	HQ5–CQ5–HQ5	38.8	109.5
CQ1–CQ2–CQ3	67.7	120.0	CR1–NR2–CR1	110.0	104.8	HQ5–CQ5–OS	35.0	109.5
CQ1–CQ2–CQ4	65.2	120.0	CR1–NR2–CR5	110.0	104.8	HQ9–CQ9–CQ10	34.1	119.9
CQ1–CQ5–CQ4	75.4	109.5	CR1–NR2–HR2	20.6	127.6	HQ12–CQ12–HQ12	38.0	109.5
CQ1–CQ5–HQ5	47.8	109.5	CR1–NR2–MG	21.6	127.6	HS4–CS4–SA1	32.80	109.5
CQ1–CT–CT	75.4	109.5	CR2–C–CT	85.0	119.2	HS4–CS4–HS4	38.78	109.5
CQ1–CT–HC	47.8	109.5	CR2–C–O	80.0	120.4	NA2–CA1–NA3	72.58	117.38
CQ2–CQ1–CQ5	75.4	109.5	CR2–CR1–CR3	60.0	122.8	NA2–CA1–NA4	72.58	117.38
CQ2–CQ1–CT	75.4	109.5	CR2–CR1–NR1	107.9	110.7	NA2–CA1–NO1	99.73	125.88
CQ2–CQ1–HQ1	48.0	109.5	CR2–CR1–NR2	107.9	110.7	NA2–CA1–NS1	107.23	125.65
CQ2–CQ3–HQ3	43.9	109.5	CR2–CR2–CR4	85.0	144.8	NA3–CA1–NO1	62.10	116.84
CQ2–CQ4–CQ5	65.2	125.0	CR2–CR2–CR5	98.5	106.8	NA3–CA1–NS1	72.92	116.87
CQ2–CQ4–HQ4	40.3	120.0	CR2–CR2–CT	70.0	125.2	NA4–CA1–NO1	62.10	116.84
CQ3–CQ2–CQ3	67.8	120.0	CR2–CR4–CT	75.0	108.3	NA4–CA1–NS1	72.92	116.87
CQ3–CQ2–CQ4	67.8	120.0	CR2–CR4–O	85.0	131.7	NB–CR–NFL	70.0	120.0
CQ4–CQ5–CQ6	75.4	109.5	CR2–CR5–CR3	60.0	114.6	NB–CR–NFU	70.0	120.0
CQ4–CQ5–HQ5	48.0	109.5	CR2–CR5–NR2	107.9	110.7	NO1–CO3–NO1	75.11	126.70
CQ4–CQ4–HQ4	34.5	115.0	CR2–CT–CT	63.0	115.6	NO1–CO3–OA1	79.28	116.65
CQ4–CQ5–OS	50.0	109.5	CR2–CT–HC	35.0	109.5	NR1–MG–NR1	18.0	180.0
CQ5–CQ1–HQ1	47.8	109.5	CR3–CR1–CT	70.0	119.7	NR1–MG–NR2	18.	90.0
CQ5–CQ6–CQ6	65.2	119.4	CR3–CR1–NR1	60.0	126.5	NR2–MG–NR2	18.	180.0
CQ5–CQ6–CQ7	65.2	119.4	CR3–CR1–NR2	60.0	126.5	NS1–CS3–NS1	89.77	126.70
CQ6–CQ5–HQ5	47.8	109.5	CR3–CR5–NR2	60.0	126.5	NS1–CS3–SA1	61.99	116.65
CQ6–CQ6–CQ7	43.6	121.2	CR3–CT–CR4	75.0	103.6	OF1–C–OF1	80.0	126.0
CQ6–CQ6–CQ12	65.2	119.4	CR3–CT–HC	35.0	109.5	O–C–OS	80.0	119.8
CQ6–CQ7–CQ8	60.4	118.8	CR4–CR2–CR5	63.0	107.0			
CQ6–CQ7–OQ7	76.5	119.7	CR4–CT–HC	35.0	109.5			

[a] For the potential $K_\theta(\theta - \theta_0)^2$ where K_θ is in kcal/mol·radian^2 and θ_0 is in deg. Other angles that are in the system and are not listed in this table have $K_\theta = 0$.

local 2-fold symmetry around the iron atom was imposed, and it was assumed that the bond-stretching modes were not significantly coupled to any other modes.

The optimized lengths for bonds between the Fe atom and the amino acid side chains were 1.96 Å for the Fe–O bond in the glutamic acid and 1.92 and 1.87 Å for the Fe–N bonds in the symmetric histidine pairs L190,M217 and L230,M264, respectively. The corresponding force constants for bond stretching were predicted to be 345, 247, and 383 kcal/mol·Å^2. We found that bending and torsional terms directly involving the Fe atom were not necessary because of dense packing brought on by 6-fold coordination: the pairwise portion of the potential accounted for these interactions. The bond, angle, and torsional parameters not directly involving the Fe atom were the same as those used in the protein. In order to distinguish the special amino acids in the force field, they were named HFL for His L190,M217, HFU for L230,M264 (NFL, NFU for the nitrogens bonded to the iron atom), and GLF for the glutamic acid M232 (OF1 for the oxygen).

The application of the ESP fitting procedure to the Fe complex was complicated by the fact that the iron atom was buried well beneath the surface of the molecule. Numerical tests on the rank[32] of the linear equations used in the least-squares fit[33] revealed that the iron atom should not be included. As a compromise, we performed the fit with the charge on iron constrained to be zero and relied upon the other atoms to effectively represent the ESP about the surface. To be consistent, the nonbonded parameters for the iron atom were also set to zero. In the simulation the Fe atom interacted with the rest of the system only through the bonds to nearest neighbors. Preliminary MD runs showed that this model was sufficient for our purposes because the positions of the atoms in this region of the protein stayed near those in the crystal.

Primary Quinone. The internal parameters for the tightly bound menaquinone Q_A were transferred directly from the diagonal elements of the valence force field for 1,4-naphthoquinone[34] and

(32) Dongarra, J. J.; Moler, C. B.; Bunch, J. R.; Stewart, G. W. *LINPACK Users' Guide*; SIAM: Philadelphia, 1979; Chapter 9.
(33) Besler, B. H.; Merz, K. M.; Kollman, P. A. *J. Comput. Chem.* **1990**, *11*, 431.
(34) Girlando, A.; Ragazzon, D.; Pecile, C. *Spectrochim. Acta* **1980**, *36A*, 1053.

Table III. Additional Torsional Parameters[a]

torsion	$V_n/2$	γ	n	torsion	$V_n/2$	γ	n
CA1-NA2-CA1-NA3	3.63	180	2	HA8-CA8-CA7-NA4	0.99	0	3
CA1-NA2-CA1-NA4	3.63	180	2	X-C-OS-X	1.45	0	3
CA1-NA2-CA1-NO1	2.29	180	2	X-CQ1-CQ2-X	1.7	0	3
CA1-NA2-CA1-NS1	2.51	180	2	X-CQ1-CQ5-X	1.7	180	2
CA1-NO1-CO3-NO1	2.64	180	2	X-CQ2-CQ3-X	0.52	0	3
CA1-NO1-CO3-OA1	5.32	180	2	X-CQ2-CQ4-X	23.6	180	2
CA1-NS1-CS3-NS1	4.83	180	2	X-CQ4-CQ5-X	1.7	180	2
CA1-NS1-CS3-SA1	6.37	180	2	X-CQ5-OS-X	1.15	0	3
CA5-NA3-CA1-NA2	3.63	180	2	X-CQ6-CQ6-X	5.3	180	2
CA5-NA3-CA1-NO1	3.63	180	2	X-CQ6-CQ7-X	5.3	180	2
CA5-NA3-CA1-NS1	3.63	180	2	X-CQ7-CQ8-X	5.3	180	2
CA7-NA4-CA1-NA2	3.63	180	2	X-CQ8-CQ8-X	5.3	180	2
CA7-NA4-CA1-NS1	3.63	180	2	X-CQ8-CQ9-X	5.3	180	2
CA7-NA4-CA1-NO1	3.63	180	2	X-CQ9-CQ10-X	5.3	180	2
CO1-OA1-CO3-NO1	2.83	180	2	X-CQ10-CQ10-X	5.3	180	2
CO3-NO1-CA1-NA2	3.83	180	2	X-CR1-NR1-X	5.6	180	2
CO3-NO1-CA1-NA3	6.52	180	2	X-CR1-CR2-X	14.3	180	2
CO3-NO1-CA1-NA4	6.52	180	2	X-CR1-CR3-X	14.3	180	2
CO3-OA1-CO4-HO4	0.72	0	3	X-CR1-NR2-X	4.8	180	2
CS3-NS1-CA1-NA2	3.05	180	2	X-CR2-C-X	1.99	0	3
CS3-NS1-CA1-NA3	5.74	180	2	X-CR2-CR2-X	14.30	180	2
CS3-NS1-CA1-NA4	5.74	180	2	X-CR2-CR4-X	1.99	0	3
CS4-SA1-CS3-NS1	3.96	180	2	X-CT-C-X	0.07	180	3
HA3-NA3-CA1-NA2	6.8	180	2	X-CT-CT-X	1.3	0	3
HA3-NA3-CA1-NO1	6.8	180	2	X-CT-CR4-X	0.07	180	3
HA3-NA3-CA1-NS1	6.8	180	2	X-CT-OS-X	1.15	0	3
HA4-NA4-CA1-NA2	6.8	180	2	X-CT-CQ1-X	1.3	0	3
HA4-NA4-CA1-NO1	6.8	180	2	X-CR-NFU-X	9.3	180	2
HA4-NA4-CA1-NS1	6.8	180	2	X-CR-NFL-X	9.3	180	2
HA5-CA5-CA6-HA6	0.30	0	3	X-CW-NFU-X	6.0	180	2
HA6-CA6-CA5-NA3	1.64	0	3	X-CW-NFL-X	6.0	180	2

[a] For the potential $(V_n/2)[1 + \cos(n\phi - \gamma)]$ where $V_n/2$ is in kcal/mol and γ is in deg. Other torsions that are in the system and are not listed in this table have $V_n/2 = 0$.

Table IV. Additional Improper Torsional Parameters[a]

torsion	$V_n/2$	γ	n	torsion	$V_n/2$	γ	n
CA1-NA3-HA3-CA4	10.5	180	2	CQ10-CQ9-CQ8-HQ9	2.0	180	2
CA1-NA3-HA3-CA5	10.5	180	2	CQ10-CQ10-CQ9-HQ10	2.0	180	2
CQ1-CQ3-CQ2-CQ4	24.7	180	2	NA2-CA1-NA4-NO1	15.43	180	2
CQ2-CQ4-CQ5-HQ4	14.3	180	2	NA2-CA1-NA4-NS1	15.09	180	2
CQ2-CQ5-CQ4-HQ4	14.3	180	2	NA3-CA1-NA2-NO1	15.43	180	2
CQ3-CQ1-CQ2-CQ4	24.7	180	2	NA3-CA1-NA2-NS1	15.09	180	2
CQ3-CQ2-CQ3-CQ4	24.7	180	2	NA4-NA2-CA1-NO1	15.43	180	2
CQ3-CQ4-CQ5-HQ4	14.3	180	2	NA4-CA1-NA2-NO1	15.43	180	2
CQ6-CQ7-CQ8-OQ7	10.5	180	2	NO1-CO3-NO1-OA1	17.83	180	2
CQ8-CQ7-CQ6-OQ7	10.5	180	2	NS1-CS3-NS1-SA1	11.74	180	2
CQ8-CQ9-CQ10-HQ9	2.0	180	2	X-OF1-C-OF1	10.5	180	2
CQ9-CQ10-CQ10-HQ10	2.0	180	2	X-X-CQ7-OQ7	10.5	180	2

[a] For the potential $(V_n/2)[1 + \cos(n\phi - \gamma)]$ where $V_n/2$ is in kcal/mol and γ is in deg. Other improper torsions that are in the system and are not listed in this table have $V_n/2 = 0$.

trans-1,4-polyisoprene.[35] These accounted for all of the necessary interactions with the exception of the torsional terms within the rings of the quinone. The proper and improper torsional force constants of Weiner et al.[16] were used to supply the missing numbers. The partial charges were computed by dividing Q_A into two separate molecules, calculating the charges, and then piecing the fragments together. The division took place where the isoprenoid tail joins the ring system. The molecule chosen to represent the ring system was a 1,4-naphthoquinone, and the one representing the isoprenoid chain contained 5 monomeric units (Figure 4). We found that, because of the electronic delocalization in the system, these many units were required to converge the calculated charges. Geometries for both of these molecules were generated by optimization with MOPAC[29] using the AM1 method. The internal coordinates of these optimized structures did not significantly deviate from experimentally determined geometries.[34]

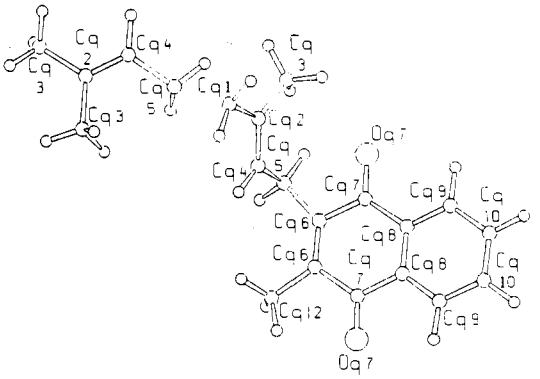

Figure 4. Atom types of the naphthoquinone and isoprene subunits of the menaquinone Q_A. Hydrogen atoms have the same suffix as the corresponding carbon atom with "C" changed to "H".

Bacteriochlorophyll *b* and Bacteriopheophytin *b*. The internal force constants for both the bacteriochlorophyll *b* (BChl-*b*) (with magnesium) and the bacteriopheophytin *b* (BPh-*b*) (without

(35) Gavish, M.; Brennan, P.; Woodward, A. E. *Macromolecules* **1988**, *21*, 2075.

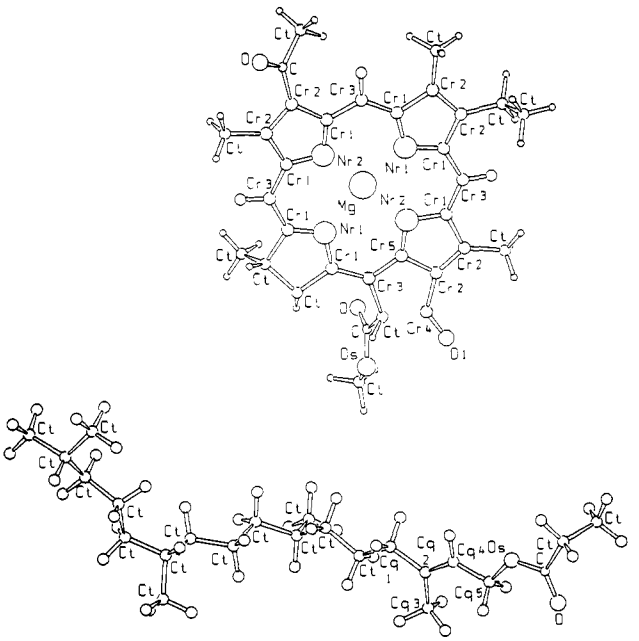

Figure 5. Atom types of the porphyrin ring system and the phytyl chain used to parametrize the bacteriochlorophyll and bacteriopheophytin molecules. Hydrogen atoms have the same suffix as the corresponding carbon atom with "C" changed to "H", with the exception of those bonded to "CT" carbons where the atom type is "HC".

magnesium) were transferred directly from the diagonal elements of porphyrin[36,37] and *trans*-1,4-polyisoprene[35] force fields. The remaining parameters were taken from similar interactions in Weiner et al.[16] Although the symmetry and corresponding normal modes of porphyrin are different from those of BChl-*b* and BPh-*b*, a comparison of their experimental geometries[38] shows that they are similar in terms of bond lengths, bond angles, and dihedral angles. The only change made to the values of Li et al.[37] was to lengthen their Ni–N bond from 1.955 Å to the crystallographically determined Mg–N distance of 2.081 Å.[38] When it was possible, the parameters given by Li et al.[37] were used instead of those given by Gladkov et al.[36] because of a few unreasonably large values of force constants reported by the latter.

The partial charges were obtained by using the ESP fitting procedure described previously. This fit was done on two separate molecules that were subsequently joined to supply the set of charges for BChl-*b* and BPh-*b*. The first molecule, aquoethyl chlorophyllide *b*, was used to model the ring system of BChl-*b* where the coordinates of the crystal structure were used in the calculations.[38] The ring system was kept intact in the computations, because we found that the electronic delocalization strongly influenced the computed partial charges. Partial charges for the BPh-*b* were also computed from this structure by adding two hydrogen atoms to the appropriate nitrogens and then removing the Mg atom. The second molecule was the phytyl chain of BChl-*b* and BPh-*b* where the coordinates used in this fit were optimized using the AM1[29] method (Figure 5).

Thermodynamic Cycle

The thermodynamic cycle used in this work is shown in Figure 6. This is essentially the same cycle as introduced by Tembe and McCammon[39] with the addition of one more substrate. This formulation allows the difference in binding free energy,

$$\Delta\Delta G^b_{ij} = \Delta G^b_i - \Delta G^b_j \quad (1)$$

to be obtained by traversing four different paths. The final $\Delta\Delta G^b_{ij}$

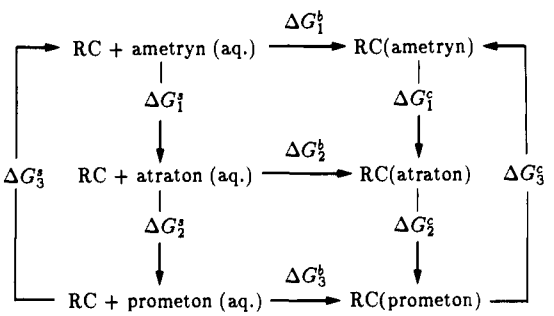

Figure 6. Thermodynamic cycle for the inhibitor–RC complexes.

values are calculated by averaging over four different paths. For example,

$$\Delta\Delta G^b_{12} = \tfrac{1}{4}((\Delta G^s_1 - \Delta G^c_1) + (-\Delta G^s_3 - \Delta G^s_2 + \Delta G^c_2 + \Delta G^c_3) + (-\Delta G^s_3 - \Delta G^s_2 - \Delta G^c_1) + (\Delta G^s_1 + \Delta G^c_2 + \Delta G^c_3)) \quad (2)$$

where ΔG^s_i and ΔG^c_i are the free energy differences between the inhibitors calculated in solvent and the RC, respectively (Figure 6). A rough measure of the uncertainty in the computation is provided by using the analogous expressions of eq 2 for $\Delta\Delta G^b_{23}$ and $\Delta\Delta G^b_{31}$ and then adding them together to obtain

$$\Delta\Delta G^b_{12} + \Delta\Delta G^b_{23} + \Delta\Delta G^b_{31} = \tfrac{1}{2}(\sum_{i=1,3} \Delta G^c_i - \sum_{i=1,3} \Delta G^s_i) \quad (3)$$

The left-hand side of eq 3 is a closed thermodynamic cycle and should equal zero. Likewise, each sum on the right-hand side of eq 3 (e.g., $\sum_{i=1,3}\Delta G^c_i$, $\sum_{i=1,3}\Delta G^s_i$) is a closed thermodynamic cycle and should also be zero. A measure of the error in the calculation can be obtained by evaluating the right-hand side of eq 3. Thus, by adding another substrate the overall cycle has the advantage of obtaining a range of uncertainty without doubling the amount of computational effort; the simulation can be done in one direction to check sampling errors.

Computational Details

The minimization, MD, and FEP calculations were carried out using the AMBER[17] suite of programs. The coordinates of *Rps. viridis* used in the simulation were the refined X-ray coordinates at 2.3-Å resolution.[40] Because of the size of the complex (~130 Å from the top of the cytochrome to the bottom of the H subunit) and the number of atoms (1187 amino acids plus cofactors), we used only a portion of the entire complex to model the inhibitor–RC interactions. The sections of the RC that were included in the simulation were chosen so that the coordinates of the model system did not significantly drift from the crystal structure throughout the course of the MD. With this in mind, we included all of the cofactors to preserve the relatively close packing of the complex and also kept the membrane-spanning helices intact even though some residues were more than 25 Å away from the site of the perturbation. The simulated model consisted of the amino acid residues L170–L250, M1–M70, M114–M162, M197–M281, and H121–H182, the four BChl-*b*'s, the two BPh-*b*'s, the Q_A, the non-heme iron, the inhibitor, and 66 crystallographic water molecules. No shell of water was soaked around the protein, because RCs are membrane-bound proteins. The entire model consisted of ~6200 atoms. The placement of the inhibitor was modeled after the X-ray structure analysis of the terbutryn–RC[12] complex.

Although Yeates et al.[41] have predicted the position and orientation of the protein in the lipid, the crystallographic data did not directly provide the positions of the lipid molecules. Because the coordinates of the lipid bilayer were not known, we did not incorporate them in the model. To compensate for the lack of the membrane, certain regions of the protein were not allowed to move throughout the simulation. These residues were in β-turns

(36) Gladkov, L. L.; Solovyov, K. N. *Spectrochim. Acta* **1985**, *41A*, 1437.
(37) Li, X.-Y.; Czernuszewicz, R. S.; Kincaid, J. R.; Su, O.; Spiro, T. G. *J. Phys. Chem.* **1990**, *94*, 31.
(38) Serlin, R.; Chow, H.-C.; Strouse, C. E. *J. Am. Chem. Soc.* **1975**, *97*, 7237.
(39) Tembe, B. L.; McCammon, J. A. *Comput. Chem.* **1984**, *8*, 281.
(40) The coordinates were kindly provided by Drs. J. Deisenhofer, H. Michel, and R. Huber.
(41) Yeates, T. O.; Komiya, H.; Rees, D. C.; Allen, J. P.; Feher, G. *Proc. Natl. Acad. Sci. U.S.A.* **1987**, *84*, 6438.

Table V. Calculated Free Energy Differences[a]

i	ΔG_i^s	$\Delta G_{i,vdw}^s$	$\Delta G_{i,ele}^s$	ΔG_i^c	
1	−0.24	0.40	−0.76	0.48	ametryn → atraton, S → O
2	−0.75	−0.07	−0.63	−0.42	atraton → prometon, H → CH_3
3	1.35	−0.22	1.79	−0.12	prometon → ametryn

[a] In kcal/mol. ΔG_i^s and ΔG_i^c were obtained by simultaneously perturbing the van der Waals and electrostatic energies while $\Delta G_{i,vdw}^s$ and $\Delta G_{i,ele}^s$ were obtained by decoupling the perturbation of the van der Waals and electrostatic energies.

Table VI. Relative Binding Free Energies[c]

	$\Delta\Delta G_{12}^b$	$\Delta\Delta G_{23}^b$	$\Delta\Delta G_{31}^b$	error
calcd[a]	−0.94	−0.54	1.26	±0.21
calcd[b]	−1.13	−0.56	1.40	±0.29
exptl	−1.12	−0.71	1.84	

[a] Computed by simultaneously perturbing the van der Waals and electrostatic energies. [b] Computed by decoupling the perturbation of the van der Waals and electrostatic energies. [c] Errors were computed by using eq 3 in the text; values in the table are in kcal/mol.

and at the ends of the membrane-spanning helices. The stationary residues were L170–L173, L201–L203, L248–L250, H1–H3, H68–H70, H114–H116, H160–H162, H197–H199, H253–H255, H279–H281, M121–M123, M149–M151, M167–M169, and M180–M182. In addition, the ring systems of the four BChl-*b*'s were kept fixed while their tails were allowed to move. This kept the histidine nitrogens bound to the Mg in the BChl-*b* through electrostatic interactions. To calculate ΔG_i^s, each inhibitor was placed inside of a box of approximately 1200 TIP3P[42] water molecules.

The initial geometries of both the inhibitor–water and inhibitor–RC systems were first minimized and then slowly warmed to a temperature of 300 K. Once they reached this temperature, they were equilibrated for 7.5 (inhibitor–water system) and 22.5 ps (inhibitor–RC systems). Here and throughout this work the SHAKE[43] algorithm was used to constrain all covalent bond distances to their equilibrium value. The integration time step was 1.5 fs, and a nonbonded cutoff length of 12 Å was used; the dielectric constant was set to 1.

For the FEP calculations, the windowing method was used.[14] Each of the ΔG_i^s and ΔG_i^c paths was taken by simultaneously perturbing the van der Waals and electrostatic potentials. The relative free energy values that we report are the contributions due to these perturbations. The entire calculation of each ΔG_i^s or ΔG_i^c was done in 21 steps with a $\Delta\lambda$ of 0.05. A total of 1000 time steps was taken for the equilibration and another 1000 time steps for the sampling at every value of λ. An additional computation was carried out by decoupling the electrostatic and van der Waals contributions along the ΔG_i^s paths.[14] Here λ was incremented by 0.001 for the van der Waals perturbation with 200 steps equilibration and 200 steps sampling. A λ increment of 0.05 was used for the electrostatic perturbation with 1000 steps equilibration and 1000 steps sampling.

Results and Discussion

The computed values for ΔG_i^s and ΔG_i^c from the individual runs are given in Table V. The calculated and experimentally determined relative binding free energies are given in Table VI. The sampling errors in these numbers are determined using eq 3 and are within the expected fluctuations of the method. The $\Delta\Delta G_{ij}^b$ values obtained through the decoupling method are slightly closer to the experimental values than those obtained by using the simultaneous perturbation method. No significance should be attached to this result because the values obtained by both methods are within sampling errors of each other. The experimental values for ΔG_i^b were obtained from the I_{50} values of the herbicides. At this concentration of the herbicide, 50% of the electron transport is inhibited. Evaluation of $\Delta G^\circ = -RT \ln K$ gives values of 7.29, 6.17, and 5.45 kcal/mol for the herbicides ametryn, atraton, and prometon, respectively. From these figures, the experimental values of $\Delta\Delta G_{ij}^b$ (in Table VI) were obtained. The agreement between the values obtained from each method is qualitative in relative binding order and quantitative within the errors and approximations involved in both of the approaches.

Unlike the current experiment, the simulation has the advantage of separating $\Delta\Delta G_{ij}^b$ into its components ΔG_{ij}^s and ΔG_{ij}^c. The ability of molecule i relative to molecule j to inhibit photosynthesis is increased by making ΔG_{ij}^c more negative and ΔG_{ij}^s more positive. This information allows the comparison of the relative importance of the free energy differences between inhibitors in the solvent and the RC to the overall binding free energy. In the thermodynamic cycle, the two chemical groups perturbed were the S → O and the H → CH_3 (Figures 2 and 6). The effects of these perturbations on the free energy differences between the inhibitors in the solvent and in the RC are discussed below.

The relative free energies of solvation (at infinite dilution) of the inhibitors in water were found to be ametryn < atraton < prometon. The perturbation of S → O shows that the oxygen-containing compound is more stable in water by ~0.24 kcal/mol, where the electrostatic and van der Waals potentials contribute ca. −0.76 and ca. 0.40 kcal/mol to the free energy difference, respectively. The electrostatic interactions probably favor the oxygen because the net charge is greater (−0.33) than on the sulfur (−0.19). This results in a larger dipole moment on the inhibitor and larger dipole–dipole interactions with water. The van der Waals interactions favor the inhibitor containing sulfur over oxygen. This could be due to rearrangements in the solvent structure around the oxygen/sulfur brought on both by different solute–solvent electrostatic interactions and by the different bond lengths to the attached carbons (Table I). The perturbation of H → CH_3 reveals that the addition of the methyl group stabilizes the solute by ~0.75 kcal/mol, with the free energy difference mostly due to electrostatic contributions (~90%).

The herbicide–RC FEP calculations yielded a ranking of the relative stabilities of the inhibitors as atraton < prometon < ametryn. In this case, the stability of the CH_3–S species over the CH_3–O species (0.46 kcal/mol) is most likely due to the hydrophobic interactions of these groups with the Leu L189 and Ile L229 residues of the RC. The marginal stability of the ametryn–RC complex over the prometon–RC complex reveals that, while the addition of the methyl group stabilizes the interactions, this stabilization is offset by the CH_3–O interactions with the hydrophobic region.

By taking the full cycle into account, two trends arise: (i) The relative free energy of solvation and relative free energy of the inhibitor–RC complexes both favor a hydrophobic group for greater binding. (ii) The addition of a methyl group to one of the compounds has competing effects: the desolvation free energy is greater (favoring the solvent), while the inhibitor–RC complex is stabilized by the methyl group (favoring the RC).

Although the results of our FEP computations are encouraging, certain limits of this work must be considered. Firstly, the model systems lacks the lipid bilayer of the membrane. Therefore, the inhibitors used in this study were chosen so that the perturbations occurred in regions that have no direct contact to the surface of the L subunit. If new inhibitors are simulated which might contact the membrane, the $\Delta\Delta G_{ij}^b$ values would be less predictable. Secondly, the free energy contributions due to internal conformational changes of the herbicides in the inhibitor–RC simulation were not taken into account. Tobias et al.[44] point out that this flexibility can influence the calculated values of free energy changes. If the conformational states accessed by the inhibitors in solution are considerably different than those accessed in the protein, these contributions should be taken into account. For-

(42) Jorgensen, W. L.; Chandrasekhar, J.; Madura, J. D. *J. Chem. Phys.* **1983**, *79*, 926.
(43) Ryckaert, J. P.; Ciccotli, G.; Berendsen, H. J. C. *J. Comput. Phys.* **1977**, *23*, 327.
(44) Tobias, D. J.; Brooks, C. L., III; Fleischman, S. H. *Chem. Phys. Lett.* **1989**, *156*, 256.
(45) Keller, E. *SCHAKAL88*; Kristallographisches Institut der Albert-Ludwigs-Universität: Freiburg, FRG, 1988.

tunately, because the triazines are relatively rigid, their conformational flexibility is limited, and thus this effect on the computed free energies might be small. Thirdly, no electronic degrees of freedom were included. Although most MD studies do not allow for different electronic states, it may be important to this system because of structural changes induced by electronic transitions.

Conclusion

Through extensive force field parameter development and the use of the MD/FEP method we were able to calculate the relative binding free energies between three triazine inhibitors of the reaction center of *Rps. viridis* prior to the experimentally determined values. The calculations quantitatively reproduce the experimental relative binding free energies of the herbicides, prometon < atraton < ametryn. There are several limitations that should be addressed in future MD simulations of the RC that include the missing lipid bilayer and the contributions of the conformational flexibility of the ligands to the free energy. These simulations allowed us to evaluate the contributions of the inhibitor substituents to the overall relative binding free energies.

Acknowledgment. We thank Drs. J. Deisenhofer, H. Michel, and R. Huber for providing the refined X-ray coordinates of the reaction center and Dr. I. Sinning for the measurement of the I_{50} values for the triazines. We also thank Dr. E. Wimmer, Dr. W. Saenger, and Dr. A. Krapoth for many fruitful discussions. We gratefully acknowledge the computational resources provided by the Corporate Computing Network at Cray Research, Inc.

Registry No. Ametryn, 834-12-8; atraton, 1610-17-9; prometon, 1610-18-0.

Supplementary Material Available: Listings of the input files to the AMBER PREP module (17 pages). Ordering information is given on any current masthead page.

Contribution of Charged Side Chains, Mg^{2+}, and Solvent Exclusion to Enzymatic β-Decarboxylation of α-Keto Acids

James H. Hurley*,† and S. James Remington†,‡

Contribution from the Institute of Molecular Biology and Department of Physics, University of Oregon, Eugene, Oregon 97403. *Received September 23, 1991*

Abstract: The origin of the enzymatic rate enhancement of one class of biochemical carbon–carbon bond cleavage reactions, metal-dependent decarboxylation at the β-carbon of an α-keto carboxylic acid, has been investigated by classical electrostatic calculations. The three-dimensional structure of the isocitrate dehydrogenase complex with Mg^{2+} and isocitrate was used to model the charge distribution in the ground and transition states in the decarboxylation reaction. The calculated transition-state stabilization by Mg^{2+} increases from −2 kcal/mol in aqueous solution to −26 kcal/mol in the low-polarizability environment of the enzyme active site. Ionized groups in the active site contribute −43 kcal/mol to binding energy but destabilize the transition state by 11 kcal/mol relative to the enzyme-bound ground state. The overall calculated transition-state stabilization of −13 kcal/mol is in reasonable agreement with the experimental rate enhancement of $>10^8$ for this enzyme class. The low polarizability of the active-site cleft is thus the major factor in enhancement of metal ion catalysis, while ionized groups of the enzyme are required to provide binding energy by stabilizing the ground state.

Introduction

The formation and cleavage of carbon–carbon bonds are of central importance in the biochemistry of all living organisms. Only a limited number of mechanisms are available under physiological conditions to carry out this type of reaction.[1] One prominent class of carbon–carbon bond-breaking reactions catalyzed by enzymes is metal-dependent decarboxylation at the β-carbon of an α-keto carboxylic acid (Figure 1). In a classic set of experiments, Westheimer and co-workers showed that this reaction is catalyzed by Mg^{2+}, Mn^{2+}, and similar ions in solution[2] but proceeds more rapidly by a factor of $>10^8$ in the presence of the enzyme.[3] Westheimer and co-workers proposed that the enzyme served two purposes: to provide substrate specificity and to act as a complexing agent to enhance the catalytic power of the metal ion. It has been suggested that the exclusion of solvent from the active site was the major factor in the enhancement of metal catalysis,[4] but this has until now not been quantitatively tested.

Electrostatic forces are the strongest noncovalent interaction available for enzyme catalysis and have been shown in several cases to play the key role in transition-state stabilization.[5-7] A finite difference solution to the Poisson–Boltzmann equation (FDPB) allows calculation of the electrostatic potential in an enzyme active site based on a realistic model which takes into account the complex shape of the protein, differences in polarizability between solvent and protein regions, and nonzero ionic strength.[8] Using the three-dimensional structure of magnesium(II) isocitrate bound to isocitrate dehydrogenase (IDH)[4,9] as a starting point for a model of the structure of the transition state, this technique has been applied to determine whether effects on the electrostatic field in the active site can account for the dramatic difference in reaction rate between enzyme and solution.

* To whom correspondence should be addressed. Telephone No. (503) 346-2367/346-5192.
† Institute of Molecular Biology.
‡ Department of Physics.

(1) Walsh, C. *Enzymatic Reaction Mechanisms*; W. H. Freeman: New York, 1979.
(2) Steinberger, R.; Westheimer, F. H. *J. Am. Chem. Soc.* **1951**, *73*, 429.
(3) Seltzer, S.; Hamilton, G. A.; Westheimer, F. H. *J. Am. Chem. Soc.* **1959**, *81*, 4018.
(4) Hurley, J. H.; Dean, A. M.; Koshland, D. E., Jr.; Stroud, R. M. *Biochemistry* **1991**, *30*, 8671.
(5) Warshel, A.; Naray-szabo, G.; Sussman, F.; Hwang, J. *Biochemistry* **1989**, *28*, 3629.
(6) Soman, K.; Yang, A.-S.; Honig, B.; Fletterick, R. *Biochemistry* **1989**, *28*, 9918.
(7) Dao-pin, S.; Liao, D.-I.; Remington, S. J. *Proc. Natl. Acad. Sci. U.S.A.* **1989**, *86*, 5361.
(8) Klapper, I.; Hagstrom, R.; Fine, R.; Sharp, K.; Honig, B. *Proteins* **1986**, *1*, 47.
(9) Hurley, J. H.; Dean, A. M.; Sohl, J. L.; Koshland, D. E., Jr.; Stroud, R. M. *Science* **1990**, *249*, 1012.

0002-7863/92/1514-4769$03.00/0 © 1992 American Chemical Society